Dysregulated Oscillatory Connectivity in the Visual System in Autism Spectrum Disorder

Seymour, R.A[1,2,3]., Rippon, G[1]., Gooding-Williams, G[1],. Schoffelen, J.M[4] & Kessler, K[1].

[1]Aston Brain Centre, School of Life and Health Sciences, Aston University, Birmingham, B4 7ET. [2]ARC Centre of Excellence in Cognition and Its Disorders, Macquarie University, Sydney, Australia, 2109. [3]Department of Cognitive Science, Macquarie University, Sydney, Australia, 2109. [4]Radboud University Nijmegen, Donders Institute for Brain, Cognition and Behaviour, Centre for Cognitive Neuroimaging, The Netherlands.

Correspondence: **Klaus Kessler** (k.kessler@aston.ac.uk)
Robert Seymour (seymourr@aston.ac.uk)

Running Title: **Visual Oscillations are Dysregulated in Autism**

Keywords: **ASD; visual system; gamma; alpha; phase-amplitude coupling; Granger causality connectivity**

Abstract

Autism Spectrum Disorder (ASD) is increasingly associated with atypical perceptual and sensory symptoms. Here we explore the hypothesis that aberrant sensory processing in ASD could be linked to atypical intra- (local) and inter-regional (global) brain connectivity. To elucidate oscillatory dynamics and connectivity in the visual domain we used magnetoencephalography (MEG) and a simple visual grating paradigm with a group of 18 adolescent autistic participants and 18 typically developing controls. Both groups showed similar increases in gamma (40-80Hz) and decreases in alpha (8-13Hz) frequency power in occipital cortex. However, systematic group differences emerged when analysing local and global connectivity in detail. Firstly, directed connectivity was estimated using non-parametric Granger causality between visual areas V1 and V4. Feedforward V1-to-V4 connectivity, mediated by gamma oscillations, was equivalent between ASD and control groups, but importantly, feedback V4-to-V1 connectivity, mediated by alpha (8-14Hz) oscillations, was significantly reduced in the ASD group. This reduction was correlated with autistic traits, indicating an atypical visual hierarchy in autism, with reduced top-down modulation of visual input via alpha-band oscillations. Secondly, at the local level in V1, coupling of alpha-phase to gamma amplitude (alpha-gamma PAC) was reduced in the ASD group. This implies dysregulated local visual processing, with gamma oscillations decoupled from patterns of wider alpha-band phase synchrony, possibly due to an excitation-inhibition imbalance. More generally, these results are in agreement with predictive coding accounts of neurotypical perception and indicate that visual processes in autism are less modulated by contextual feedback information.

Introduction

Autism Spectrum Disorder (ASD) is a neurodevelopmental condition, characterised by impairments in social interaction, communication and repetitive behaviours (1). Although these features remain the primary diagnostic markers of ASD, the presence of sensory symptoms have recently been given a more central role, consistent with reports that over 90% of ASD individuals experience hyper- and/or hypo-sensitive responses during sensory perception (2). Alterations to low-level sensory systems may also contribute to atypical developmental trajectories of higher-level cognitive functions in autism (3). An understanding of the neural circuits involved will therefore prove fruitful for ASD research, and could even provide early diagnostic markers (4, 5).

Dysregulated neural oscillations – rhythmical changes in neural activity – are a promising neural correlate of atypical sensory processing in autism. Early electrophysiological work suggested that autistic-style perception was linked with increased gamma band power (>30Hz) in response to illusory figures and faces (6, 7). This was interpreted as an inability to synchronise visual responses at gamma frequencies, and bind perceptual processes into a coherent whole (8). Within the alpha-band (8-13Hz), reduced oscillatory synchronisation has been reported (9), which could reflect an inability to regulate widespread inhibitory processes and modulate sensory perception (4, 10). However, findings regarding differences in gamma and alpha-band power in autism, remain inconclusive overall, with both increases and decreases reported (reviewed in (4, 10). We suggest that these

inconsistencies might be reconciled by shifting the focus from oscillatory power towards considering the oscillation-mediated functional connectivity at the global and local scales (4, 10).

Functional connectivity has been proposed as a unifying framework for autism, with the predominant theory emerging from fMRI data being a global reduction but local increase in connectivity (11, 12). Recent M/EEG research has supported the first of these claims with reductions in global connectivity during set-shifting, slit-viewing, face processing and whole-brain resting state studies (13–16). These reductions in connectivity are generally tied to feedback processes, located within the frontal lobes, and mediated by oscillations in theta (3-6Hz), alpha (8-13Hz) and beta-bands (13-30Hz). Interestingly, a recent study showed that during somatosensory stimulation, feedforward connectivity from primary to secondary somatosensory cortex is increased in ASD (17). This suggests that feedforward pathways in the autistic brain may be over-compensating for the lack of feedback connectivity. At the local level, M/EEG studies have not supported the local increase in connectivity reported using fMRI (18). An emerging biologically-relevant proxy for local connectivity is the coupling of oscillations from different frequency-bands, termed cross-frequency coupling (19, 20). In particular, phase-amplitude coupling (PAC) has been proposed to act as a mechanism for the dynamic co-ordination of brain activity over multiple spatial scales, with the amplitude of high-frequency activity within local ensembles coupled to large-scale patterns of low-frequency phase synchrony (21). Alpha-gamma PAC is also closely tied to the balance between excitatory and inhibitory (E-I) populations of neurons (22), which is affected in autism (23). One previous study has reported dysregulated alpha-gamma PAC in the fusiform face area during emotional face processing in autistic adolescents (14). Local PAC was also related to patterns of global alpha hypoconnectivity in autism, suggesting that local and global connectivity are concurrently affected. Altogether, oscillation-based functional connectivity in autism is characterised by local dysregulation and global hypoconnectivity (4).

Within the context of visual processing, this view leads to several hypotheses, outlined in (4). Electrocorticography (ECoG) recordings in macaques and MEG in humans have shown that visual oscillations in different frequency bands have distinct cortical communication profiles. Gamma-band oscillations pass information up the visual hierarchy, in a feedforward manner, whereas alpha and beta-band oscillations mediate feedback connectivity, down the cortical hierarchy (24, 25). Long-range alpha/beta connectivity has also been linked with top-down attentional processes during visual perception via the regulation of local gamma oscillations (26, 27) and of local alpha-gamma PAC (28). If autism is associated with alterations in directed functional connectivity (17), we hypothesise reduced feedback connectivity within the visual system, mediated by oscillations in the alpha band, but potentially increased feedforward connectivity in the gamma band (4). At the local level, neurotypical visual processing is accompanied by increases in alpha-gamma PAC, thought to arise through the E-I coupling between infragranular and supragranular layers of visual cortex (29). Given an E-I imbalance in autism and reported local dysregulation of cortical activity, we hypothesise reduced alpha-gamma PAC within primary visual cortex (4, 14). Finally, if top-down alpha connectivity has a modulatory effect on bottom-up processing, then local alpha oscillations and alpha-gamma PAC, e.g. in V1, should reveal a systematic relationship with top-down alpha connectivity, e.g.

from V4 (14). However this may present itself differently between groups, with a more variable relationship between feedback connectivity and local PAC in the ASD group (30).

We tested these hypotheses using MEG, which combines excellent temporal resolution with sophisticated source localisation techniques (31, 32). A group of 18 adolescent ASD participants and 18 typically developing controls performed an engaging visual task, to induce alpha and gamma oscillations. We characterised changes in power and connectivity between visual areas V1 and V4: two regions with strong hierarchical connectivity (33). Additionally, we quantified local alpha-gamma PAC for V1 (20).

Methods and Materials

Participants

Data were collected from 18 participants diagnosed with ASD and 18 age-matched typically developing controls, see Table 1. ASD participants had a confirmed clinical diagnosis of ASD or Asperger's syndrome from a paediatric psychiatrist. Participants were excluded if they were taking psychiatric medication or reported epileptic symptoms. Control participants were excluded if a sibling or parent was diagnosed with ASD. Data from a further 9 participants were excluded, see *Supplementary Methods.*

	N	Age	Male/Female	Autism Quotient (Adult)	Raven Matrices Score	Glasgow Sensory Score	Mind in the Eyes Score
ASD	18	16.67	14 male; 4 female	32.6*	43.8	65.3*	21.8
Control	18	16.89	15 male; 3 female	10.9	48.7	38.7	25.4

Table 1: Participant demographic and behavioural data. * = behavioural scores significantly greater in ASD>control group, t-test, p<.05.

Experimental Procedures

Experimental procedures complied with the Declaration of Helsinki and were approved by Aston University, ethics committee. Participants and a parent/guardian gave written informed consent.

Behavioural Assessments

General non-verbal intelligence was assessed using the Raven's Matrices Task (34). The severity of autistic traits was assessed using the Autism Quotient (AQ) and sensory traits using the Glasgow Sensory Questionnaire (GSQ) (35). AQ and GSQ scores were significantly higher in the ASD group (Table 1). Participants also completed the Mind in the Eyes test (36), however, there were no group differences. The Mind in the Eyes test has been criticised for measuring emotion recognition rather than an autism-specific deficit in mental state attribution (37), and therefore these scores were not analysed further.

Paradigm

Whilst undergoing MEG, participants performed a sensory task (Figure 1A), designed to elicit gamma-band oscillations. Each trial started with a randomised fixation period (1.5, 2.5 or 3.5s), followed by the presentation of a visual grating or auditory binaural click train stimulus; however only visual data will be analysed in this article. The visual grating had a spatial frequency of 2 cycles/degree and was presented for 1.5s. To promote task engagement, cartoon pictures of aliens or astronauts were presented after the visual grating, for 0.5s but did not form part of the MEG analysis. Participants were instructed to respond to the appearance of an alien picture using a response pad (maximum response period of 1.5s). The accuracy of the response was conveyed through audio-visual feedback, followed by a 0.5s fixation period. MEG recordings lasted 12-13 minutes and included 64 trials with visual grating stimuli. Accuracy rates were above 95% for all participants.

MEG and MRI Acquisition.

MEG data were acquired using a 306-channel Neuromag MEG device (Vectorview, Elekta, Finland). A structural T1 brain scan was acquired for source reconstruction using a Siemens MAGNETOM Trio 3T scanner. MEG sensors were co-registered with anatomical MRI data by matching the digitised head-shape data with surface data from the structural scan (38). For each participant, a cortical mesh was constructed using Freesurfer v5.3 (39), and registered to a standard fs_LR mesh (Van Essen 2012). For more detailed instructions, see *Supplementary Methods.*

MEG Pre-Processing

MEG data were pre-processed using Maxfilter (tSSS, .9 correlation), which supresses external sources of noise (41). Further pre-processing was performed in Matlab 2014b using the Fieldtrip toolbox v20161024 (42). Data were band-pass filtered (0.5-250Hz, Butterworth filter) and band-stop filtered (49.5-50.5Hz; 99.5-100.5Hz) to remove power-line contamination and harmonics. Data were epoched into segments of 4s (1.5s pre, 1.5s post stimulus onset, with ±0.5s padding), demeaned and detrended. Trials containing artefacts (SQUID jumps, eye-blinks, head movement, muscle) were removed if the trial-by-channel magnetomer variance exceeded $8x10^{-23}$, resulting in removal of 3.1 trials on average per participant. Four noisy MEG channels were removed from all analyses.

Source-Level Power

Source analysis was conducted using a linearly constrained minimum variance beamformer (32), which applies a spatial filter to the MEG data at each vertex of the cortical mesh. Due to differences in noise between sensor-types, covariance matrix terms resulting from multiplying magnetomer and gradiometer data were removed. Beamformer weights were calculated by combining this covariance matrix with leadfield information, with data pooled across baseline and grating periods. Following tSSS, sensor-level data had a rank 64 or below, and therefore a regularisation parameter of lambda 5% was applied. Data were band-pass filtered between 40-80Hz (gamma) and 8-13Hz (alpha), and source analysis was performed separately. To capture induced rather than evoked visual power, a period of 0.3-1.5s following stimulus onset was compared with a 1.2s baseline period (1.5-0.3s before grating onset).

ROI definition

To quantify directed connectivity within the visual system, we selected two regions of interest (ROI): visual area 1 (V1) and visual area 4 (V4), defined using HCP-MMP 1.0 atlas (43) (Figure 1C). Both regions show stimulus-related changes in oscillatory power (Figure 1E-F) and demonstrate reliable patterns of hierarchical connectivity: V1-to V4 connectivity is feedforward; whereas V4-to-V1 connectivity is feedback (24, 25, 33). 12 vertices from posterior V1 were excluded to ensure clear anatomical separation of the ROIs. To obtain a single spatial filter for each ROI, we performed a principal components analysis on the concatenated filters encompassing V1 and V4, multiplied by the sensor-level covariance matrix, and extracted the first component (44). Broadband (0.5-250Hz) sensor-level data was multiplied by this spatial filter to obtain "virtual electrodes". Finally, the change in oscillatory power between grating and baseline periods was calculated using multi-tapers (45) from 1-140Hz, 0.5s time window, sliding in steps of 0.02s and ±8Hz frequency smoothing.

V1-V4 Directed Connectivity

To quantify V1-V4 directed functional connectivity, we used a spectrally resolved non-parametric version of Granger Causality (GC) – a statistical technique which measures the extent to which one time series can predict another (46, 47). Data from V1 and V4 (0.3-0.1.5s post-stimulus onset) were split into 0.4s epochs to enhance the accuracy of results, Fourier transformed (Hanning taper; 2Hz smoothing), and entered into a non-parametric spectral matrix factorisation procedure. GC was then estimated between 1-140Hz for each ROI pair and averaged across hemispheres. Scrambled time-series with the same spectral properties as V1/V4 were created for comparison, modelled using the first autoregressive coefficient (48), and the above steps were repeated.

Asymmetries in GC values were quantified using a Directed Asymmetry Index (DAI), see below (24).

$$DAI = \frac{GC(V1 \rightarrow V4) - GC(V4 \rightarrow V1)}{GC(V1 \rightarrow V4) + GC(V4 \rightarrow V1)}$$

This results in normalised values (-1 to +1) for every frequency bin, with values above 0 indicating feedforward GC influence and values below 0 indicating feedback influence. DAI values were statistically compared between groups.

Phase-Amplitude Coupling (PAC)

V1 time courses were examined for changes in alpha-gamma PAC. For detailed discussion about PAC computation and methodological issues see (20). Briefly, we calculated PAC between 7-13Hz phase (1Hz steps) and amplitudes 34-100Hz (in 2Hz steps), from 0.3-1.5s post-grating presentation. PAC values were corrected using 1.2 of data from the baseline period. This resulted in 33*7 amplitude-phase comodulograms, which were statistically compared between groups (49).

To calculate PAC values, we used a mean vector length approach (50), see *Supplementary Methods*, based on our previous study which compared the efficacy of four different PAC algorithms (20). We repeated the analysis with a phase-locking value approach (51), see Figure S3. Code used for PAC computation is available at: https://github.com/neurofractal/sensory_PAC.

Statistical Analysis

Statistical analysis was performed using cluster-based permutation tests (49), which consist of two parts: first an independent-samples t-test is performed, and values exceeding an uncorrected 5% significance threshold are grouped into clusters. The maximum t-value within each cluster is carried forward. Second, a null distribution is obtained by randomising the condition label (e.g. ASD/control) 1000 times and calculating the largest cluster-level t-value for each permutation. The maximum t-value within each original cluster is then compared against this null distribution, and the null hypothesis is rejected if the test statistic exceeds a threshold of p<.05.

Results

Oscillatory Power

The change in oscillatory power following presentation of the visual grating was calculated on a cortical mesh for the alpha (8-13Hz) and gamma (40-80Hz) bands. For both ASD and control groups there was a statistically significant increase in gamma power (Figure 1B) and a decrease in alpha power (Figure 1C), localised to the ventral occipital cortex. This replicates previous MEG/EEG studies using visual grating stimuli (25, 45, 52). Interestingly, there were no significant differences in gamma or alpha power between groups (p>.05, Figure S1).

Two regions of interest (ROI) were defined in V1 and V4 (Figure 1D). Changes in oscillatory power from V1 (Figure 1E) and V4 (Figure 1F) showed characteristic increases in gamma-band power (40-80Hz) and decreases in alpha/beta power (8-20Hz). Between groups, there were minor differences between the power spectra, including a larger alpha/beta induced power change for the ASD group (Fig 2E, 2F, purple line), however none of these differences was significant (both p>.05).

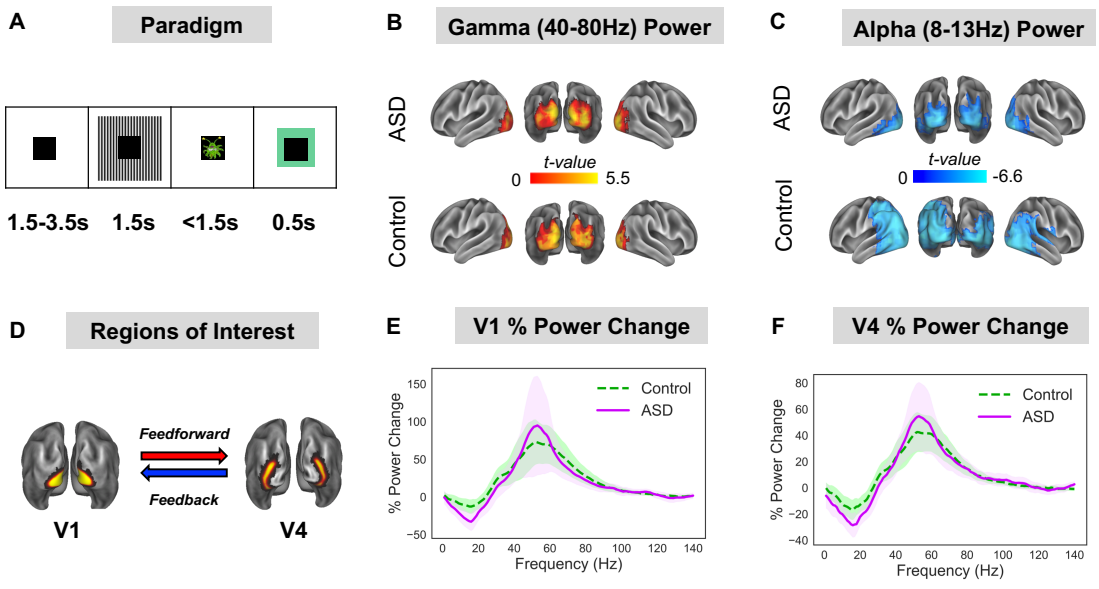

Figure 1: (A) Participants performed a visual task, consisting of 1.5-3.5 baseline period followed by 1.5s presentation of a visual grating. After the

grating, participants were presented with a cartoon alien or astronaut picture and instructed to only respond when an alien was presented (response time up to 1.5s). The alien/astronaut stimuli were to maintain attention and do not form part of the analysis. (B-C) The change in oscillatory power between grating and baseline periods was localised on a cortical mesh, and masked to show only statistically significant (p<.05, corrected) stimulus induced increases in gamma (40-80Hz) and deceases in alpha (8-13Hz) power. There were no statistically significant differences in gamma or alpha power between groups. (D) Regions of interest in V1 and V4 were defined using HCP-MMP 1.0 atlas (43). (E-F) The change in power between grating and baseline periods was calculated for V1 and V4 from 1-140Hz. Results show characteristic reductions in alpha/beta power and increases in gamma-band power (40-80Hz) for V1 and V4. There were no statistically significant differences in power between groups. The shaded area around each curve indicates 95% confidence intervals.

Feedforward / Feedback Connectivity

The directed functional connectivity between V1-V4 was quantified using Granger Causality (GC). Across groups, all reported increases in bidirectional V1-V4 GC were greater than for scrambled data (Figure S2). For the control group (Figure 2A), V1-to-V4 (henceforth termed feedforward) connectivity showed a prominent increase from 40-80Hz in the gamma band. In contrast, V4-to-V1 (henceforth termed feedback) connectivity showed a prominent increase from 8-13Hz in the alpha band (Figure 2A). This dissociation between feedforward gamma and feedback alpha, replicates previous findings in macaques and humans (24, 25). The feedforward gamma-band peak (40-80Hz) was also evident in the ASD Granger spectra (Figure 2B, red line). However, there was a reduction in the alpha-band feedback peak in the ASD group compared with controls (Figure 2B, blue line).

To quantify asymmetries in feedforward/feedback connectivity between groups, we calculated the directed asymmetry index (DAI, see *Materials and Methods*). The control group displayed a feedback peak from 0-20Hz (negative DAI values) and feedforward peak from 40-80Hz (positive DAI values). By statistically comparing DAI between groups, it was found that values from 8-14Hz were significantly lower (p=.032) for the control group than the ASD group. All other frequencies, including gamma (40-80Hz) showed similar DAI values between groups. This suggests reduced V4-to-V1 feedback connectivity for the ASD group, mediated by alpha-band oscillations (8-14Hz), but typical V1-to-V4 feedforward connectivity mediated by gamma oscillations (40-80Hz).

There was no feedforward Granger causality peak in the theta-band (4-8Hz) for either the control or ASD group, as previously reported using ECoG (53). This could be due to lower sensitivity of MEG recordings (25), as well as the centrally-masked visual grating (Fig. 1A).

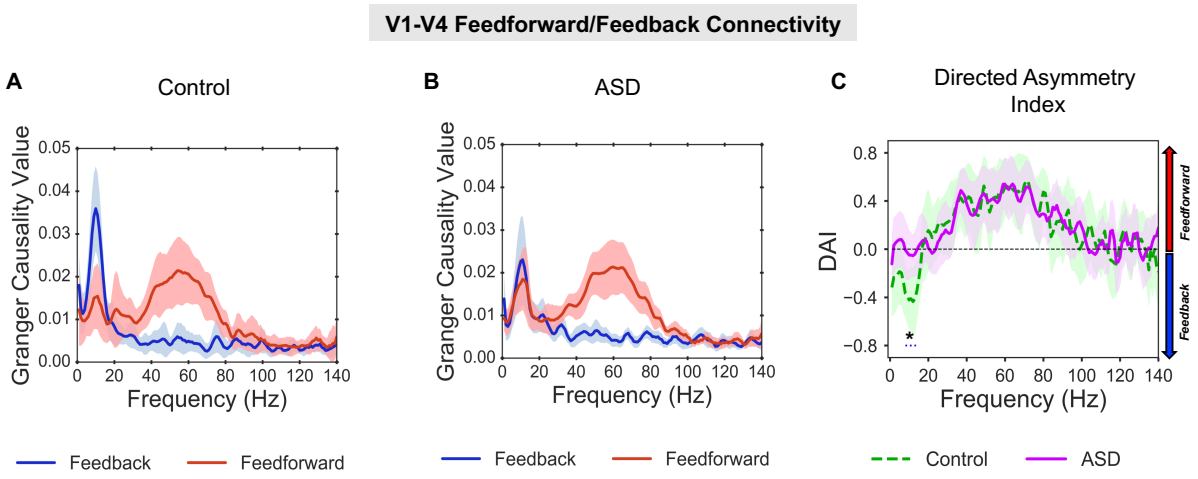

Figure 2. V1-V4 Feedforward/Feedback Connectivity. (A) For the control group there was a peak in granger causality (GC) values, in the gamma-band (40-80Hz, red line) for V1-to-V4 feedforward connectivity, and a peak in GC values in the alpha band (8-14Hz, blue line) for V4-to-V1 feedback connectivity. (B) For the ASD group there was also a peak in GC values in the gamma-band for V1-to-V4 feedforward connectivity, however there was smaller peak in GC in the alpha-band for V4-to-V1 feedback connectivity. (C) The difference between feedforward and feedback connectivity was quantified as the directed asymmetry index (DAI, see Material and Methods). The difference in DAI between control (dashed, green line) and ASD (solid, purple line) was significant (p=.036), with lower DAI values (p=.036) between 8-14Hz for the control group, suggesting reduced V4-to-V1 feedback connectivity in autism. The shaded area around each GC line indicates 95% confidence intervals.

Alpha-Gamma Phase Amplitude (PAC) in V1

Activity from visual area V1 was examined for changes in alpha-gamma PAC. Frequency comodulograms showed increased PAC in the control group, peaking at 8-10Hz phase frequencies and 50-70Hz amplitude frequencies (Figure 3A). These results replicate (20), who showed increased alpha-gamma PAC in an adult population using the same visual grating stimulus. The comodulograms for the ASD group display lower PAC values, with no clear positive peak (Figure 3B). Comparing control vs. ASD groups, there was a single positive cluster of greater PAC between 8-9Hz and 52-74Hz (p=.029). This suggests that the coupling between alpha and gamma oscillations in primary visual cortex, during perception, is reduced in autism. An alternative method for PAC computation, based on the phase locking value, produced similar comodulograms (Figure S3).

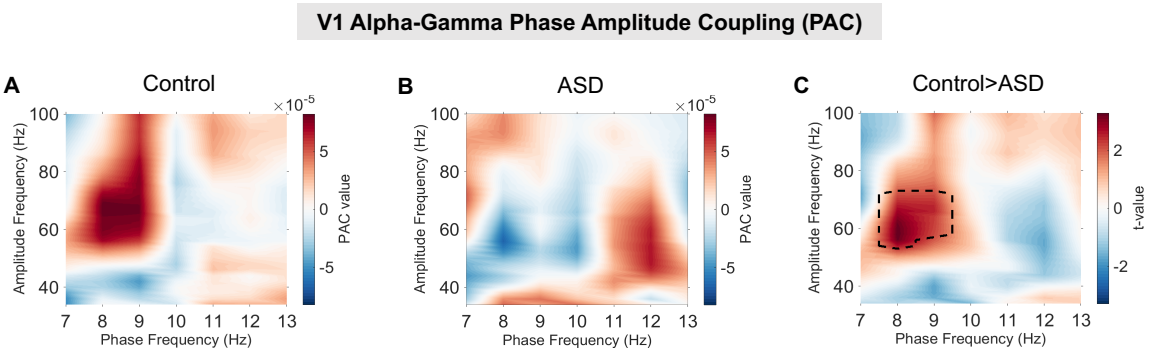

Figure 3. V1 Phase Amplitude Coupling. (A) The control group showed increased alpha-gamma PAC compared with baseline, with a peak between 50-80Hz amplitude and 7-9Hz phase. (B) The ASD group showed less prominent increases in PAC with a much smaller peak from 40-70Hz amplitude and 11-13Hz phase. (C) Statistical comparison of control>ASD indicated significantly larger PAC for the control group (p=.029) from 54-72Hz amplitude and 8-9Hz phase.

Feedback - PAC Correlation

To investigate the relationship between feedback and local processing, we ran an exploratory correlation analysis between alpha-band feedback connectivity (DAI 7-13Hz) and V1 PAC. Pooling the data from both subject groups there was a negative correlation between 9Hz DAI and 8Hz PAC, (Figure 4, Pearson's r =-.35, p =.034, uncorrected for multiple comparisons across the cross-correlation matrix) suggesting that increased V4-to-V1 feedback connectivity is related to greater local PAC in V1. Upon closer inspection, the two groups contributed quite differently to the correlation. The majority of control participants are located in the top-left quadrant of Fig. 4B, whereas the majority of ASD participants were outside this top-left quadrant. The frequency distribution across the four quadrants was significantly different between the two groups as revealed by a further Chi-Square test (chisq=7.99; p=.046), differing most strongly in the top-left (control: 13; ASD: 5) and bottom-right (control: 1; ASD: 6) quadrants.

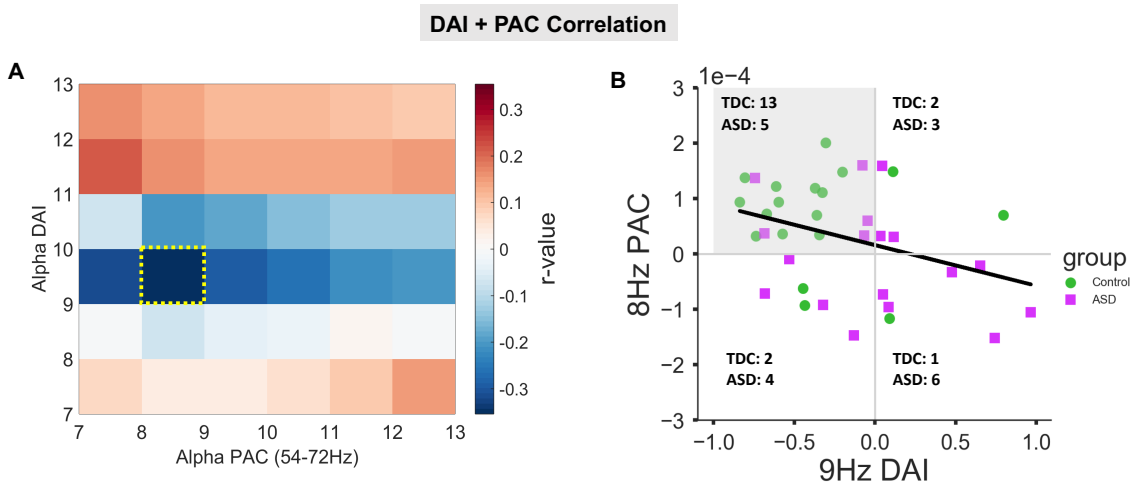

Figure 4. (A) To investigate the correlation between feedback connectivity and PAC, a cross correlation matrix was calculated in 1Hz steps between ASD and control participant's alpha PAC, averaged between 54-72Hz, and 7-13Hz directed asymmetry index (DAI). This produced a negative correlation peak, shown with yellow box, at 8Hz PAC, 9Hz DAI. (B) The correlation between 8Hz PAC, 9Hz DAI is negative across both groups (Pearson's r = -.35, p = .034). Note that only the top-left quadrant reflects the relationship postulated for effective processing: feedback alpha in form of negative DAI values (x-axis) paired up with positive PAC values (y-axis). 13 out of 18 control participants but only 5 out of 18 ASD participants are located in this quadrant (frequencies per group are indicated for each quadrant). Further explanations in text.

Connectivity - Behaviour Correlation

Behavioural ASD data from the Autism Quotient (AQ) and Glasgow Sensory Questionnaires (GSQ) were correlated with group differences in alpha-band DAI and alpha-gamma PAC (Figure 5). There was a significant positive correlation between AQ score and alpha DAI (Figure 5B, r=.526, p=.025) suggesting that increased V4-to-V1 feedback connectivity (negative DAI values) is related to lower levels of autistic traits (lower AQ scores). There were no other significant correlations for the GSQ or PAC.

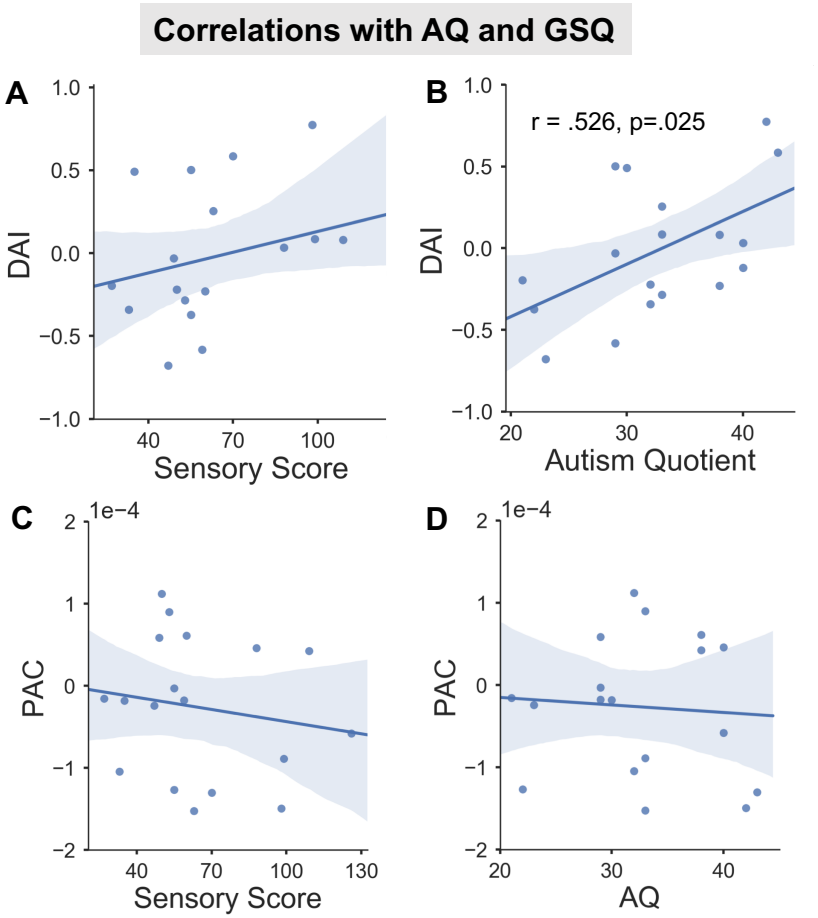

Figure 5: For the ASD group, the correlation between alpha-band DAI (A-B), alpha-gamma PAC (C-D) and Autism Quotient (B,D), Glasgow Sensory Score (A,C) was plotted with regression line (95% confidence interval indicated by shaded region). (B) There was a positive correlation between DAI and AQ score.

Discussion

This study examined the oscillation-based functional connectivity within the visual system of autistic adolescents and typically developing age-matched controls. Confirming our hypotheses (4), we found a reduction in alpha-band (8-14Hz) feedback connectivity from V4-to-V1 in the ASD group, which was positively correlated with autistic traits. Additionally, there was a reduction in the coupling between alpha and gamma oscillations in V1, measured via PAC, suggesting dysregulation of local connectivity in autism.

Feedback / Feedforward Connectivity

The reduction in feedback connectivity is consistent with previous MEG and fMRI studies showing a reduction in global connectivity in autism (12, 14, 15). In this instance, a simple visual paradigm showed that the reduction in connectivity was specific to alpha-band oscillations from 8-14Hz (Figure 2). Alpha oscillations underlie the functional inhibition and disengagement of task-irrelevant brain regions,

promoting information flow through precise timing of neural activity (26). Posterior alpha-band activity is also a mechanism for top-down modulation of perceptual processes, linked with spatial attention and phase-locking with wider frontoparietal control networks (54, 55). Our data suggest that in autism, whilst alpha power is unaffected, the feedback flow of information from higher to lower visual regions is reduced. An inability to implement top-down modulation of bottom-up visual information, may result in the atypical sensory processes reported by autistic persons and contribute to the severity of symptoms more generally (4, 10). In support of this, we found a correlation between the reduction in feedback connectivity and AQ score.

Interestingly, we did not find an increase in connectivity from V1-to-V4 for the ASD group mediated by gamma oscillations, suggesting typical feedforward flow of visual information. Whilst Khan and colleagues reported increased feedforward connectivity in autism (17), they focussed on somatosensory rather than visual processing with a younger group of adolescent participants. In any case, we hypothesise that where perception can be achieved via feedforward processes (56), autistic participants will perform on par or even outperform their typically developing peers (57); for example during visual search tasks, where autistic participants perform faster than controls (58).

PAC

Within primary visual cortex, there was a reduction in alpha-gamma PAC for the ASD group (Figure 3). Reduced alpha-gamma PAC in autism has previously been reported during emotional face perception in the fusiform gyrus (14), and during rest (59). This suggests that increases in local gamma power, driven by visual input, are decoupled from wider patterns of top-down alpha-band connectivity in autism. As PAC relies heavily on local inhibitory populations of neurons (60), a reduction in PAC is consistent with histological findings showing underdeveloped inhibitory interneurons (61), and an E-I imbalance in autism (23). Where local inhibitory processes are affected, this would manifest as high-frequency ‘noisy’ activity in the brain, common in ASD (61), and reduced signal-to-noise (23). It is important to note that the group differences in PAC arose despite similar changes in gamma and alpha power (Figure 1). Interestingly, one previous ASD study reported reduced global connectivity and local PAC despite similar event-related activity and oscillatory power between groups (14). Future studies should therefore explore the precise regulation of gamma oscillations via cross-frequency coupling, rather than relying on measures of power alone (4, 10).

Dysregulated local activity could also have concomitant effects on establishing patterns of global connectivity in autism (62). Indeed, there was a correlation between feedback connectivity and the strength of PAC across groups (Figure 4), see (14). However, whilst the control group showed increased feedback alpha and increased alpha-gamma PAC, the relationship for the ASD group was much more variable (Figure 4B). This is consistent with recent findings suggesting that brain connectivity and evoked responses are idiosyncratic in autistic samples, perhaps reflecting atypical neurodevelopmental trajectories and dysregulated local activity (30, 63).

Interestingly, we did not find a relationship between AQ or GSQ and PAC in the ASD group (Figure 5D). In contrast, a recent study reported a correlation between Autism Diagnostic Observation Schedule (ADOS) social score and local PAC in an adolescent autistic sample (64), suggesting that PAC may be related to clinical features of autism rather than general autistic traits (see *Limitations*).

Neurocognitive Models of Perception in ASD

More generally, our results link with emerging theories of perception in autism. Predictive-coding accounts of cortical activity describe the passage of top-down predictions from higher to lower areas via feedback pathways, with prediction errors computed at each level of the hierarchy being passed forward via feedforward pathways (65). Predictive-coding accounts of autism suggest that differences in perception emerge from fewer or hyper-precise top-down predictions, such that perception is less influenced by prior knowledge and contextual cues (66, 67). Our data clearly support this proposal by showing reduced feedback connectivity in the visual cortex in autism. This suggests that autistic perception can be characterised by differences in the hierarchical passage of information flow (66), captured through measures of oscillatory coupling. Where top-down information flow is reduced, this would force the perceptual system from predictive to reactive, with increased prediction error signalling and concomitant impacts on autistic symptoms (4). This is supported by the observed correlations between feedback connectivity and PAC (Figure 4) and feedback connectivity and AQ score (Figure 4B).

Clinical Implications, Limitations, and Future Work

We note two limitations to this study. First, we did not collect a formal clinical assessment of autism, e.g. the ADOS. We therefore implemented strict participant exclusion criteria, only including autistic participants with a confirmed clinical diagnosis of ASD or Asperger's syndrome. Between groups, there were significant differences in autistic and sensory traits (Table 1). However, upon closer inspection of GSQ data, the ASD group showed a mixture of hyper- and hypo-sensitive traits between different sensory modalities making precise brain-behavioural correlations problematic (Figure S4). This may explain the lack of relationship between oscillatory connectivity and GSQ scores in autism (Figure 5A, C). Brain-behaviour relationships might be better assessed using psychophysical tests of visual perception (68), combined with formal clinical assessments. Second, we constrained our connectivity analyses to two regions of interest (V1, V4) located early in the visual system, due to their hierarchical connectivity, and the low-level nature of the visual grating stimulus. However, we may have missed the opportunity to characterise more complex feedforward-feedback relationships in wider visual cortex. Future work should therefore include more ROIs in combination with stimuli requiring participants to explicitly engage in feedback processing to constrain visual perception. This approach could be particularly useful with high-functioning individuals, and help characterise the neurophysiological basis of autistic perception (3, 4).

The current results indicate that measures of oscillatory connectivity within the visual system, can elucidate atypical neural mechanisms in the autistic brain. Future research should elaborate on the current work by assessing these connectivity measures for their potential as stratification biomarkers of ASD in high-powered longitudinal studies (69). Due to the simplicity of the employed stimulus, the paradigm presented here could even be used in paediatric or non-verbal

populations, since passive viewing of simple grating stimuli is sufficient for extracting the presented connectivity measures.

Acknowledgments

We wish to thank: the volunteers who gave their time to participate in this study; Dr. Shu Yau for help with MRI data acquisition; Dr. Jon Brock for intellectual contributions to experimental design; and the Wellcome Trust, Dr Hadwen Trust and Tommy's Fund for supporting research costs. Robert Seymour was supported by a cotutelle PhD studentship from Aston University and Macquarie University. Jan-Mathijs Schoffelen was supported by The Netherlands Organisation for Scientific Research (NWO Vidi: 864.14.011).

References

1. American Psychiatric Association (2013): Diagnostic and statistical manual of mental disorders. *Arlingt Am Psychiatr Publ*.
2. Leekam SR, Nieto C, Libby SJ, Wing L, Gould J (2007): Describing the sensory abnormalities of children and adults with autism. *J Autism Dev Disord*. 37: 894–910.
3. Robertson CE, Baron-Cohen S (2017): Sensory perception in autism. *Nat Rev Neurosci*. 18: 671.
4. Kessler K, Seymour RA, Rippon G (2016): Brain oscillations and connectivity in autism spectrum disorders (ASD): new approaches to methodology, measurement and modelling. *Neurosci Biobehav Rev*. 71: 601–620.
5. Roberts TP, Khan SY, Rey M, Monroe JF, Cannon K, Blaskey L, *et al.* (2010): MEG detection of delayed auditory evoked responses in autism spectrum disorders: towards an imaging biomarker for autism. *Autism Res*. 3: 8–18.
6. Brown C, Gruber T, Boucher J, Rippon G, Brock J (2005): Gamma abnormalities during perception of illusory figures in autism. *Cortex*. 41: 364–376.
7. Sun L, Grützner C, Bölte S, Wibral M, Tozman T, Schlitt S, *et al.* (2012): Impaired gamma-band activity during perceptual organization in adults with autism spectrum disorders: evidence for dysfunctional network activity in frontal-posterior cortices. *J Neurosci*. 32: 9563–9573.
8. Brock J, Brown CC, Boucher J, Rippon G (2002): The temporal binding deficit hypothesis of autism. *Dev Psychopathol*. 14: 209–224.
9. Milne E, Scope A, Pascalis O, Buckley D, Makeig S (2009): Independent Component Analysis Reveals Atypical Electroencephalographic Activity During Visual Perception in Individuals with Autism. *Biol Psychiatry*, Perception, Empathy, and Reward in Attention-Deficit/Hyperactivity Disorder and Autism. 65: 22–30.
10. Simon DM, Wallace MT (2016): Dysfunction of sensory oscillations in Autism Spectrum Disorder. *Neurosci Biobehav Rev*. 68: 848–861.
11. Courchesne E, Pierce K (2005): Why the frontal cortex in autism might be talking only to itself: local over-connectivity but long-distance disconnection. *Curr Opin Neurobiol*. 15: 225–230.
12. Hughes JR (2007): Autism: the first firm finding= underconnectivity? *Epilepsy Behav*. 11: 20–24.
13. Doesburg SM, Vidal J, Taylor MJ (2013): Reduced Theta Connectivity during Set-Shifting in Children with Autism. *Front Hum Neurosci*. 7.
14. Khan S, Gramfort A, Shetty NR, Kitzbichler MG, Ganesan S, Moran JM, *et al.* (2013): Local and long-range functional connectivity is reduced in concert in

584 autism spectrum disorders. *Proc Natl Acad Sci*. 110: 3107–3112.
585 15. Kitzbichler MG, Khan S, Ganesan S, Vangel MG, Herbert MR, Hämäläinen MS,
586 Kenet T (2015): Altered Development and Multifaceted Band-Specific
587 Abnormalities of Resting State Networks in Autism. *Biol Psychiatry*, Autism
588 Genotypes and Phenotypes. 77: 794–804.
589 16. Peiker I, David N, Schneider TR, Nolte G, Schöttle D, Engel AK (2015):
590 Perceptual Integration Deficits in Autism Spectrum Disorders Are Associated
591 with Reduced Interhemispheric Gamma-Band Coherence. *J Neurosci*. 35:
592 16352–16361.
593 17. Khan S, Michmizos K, Tommerdahl M, Ganesan S, Kitzbichler MG, Zetino M, *et*
594 *al.* (2015): Somatosensory cortex functional connectivity abnormalities in
595 autism show opposite trends, depending on direction and spatial scale. *Brain*.
596 138: 1394-1409.
597 18. Keown CL, Shih P, Nair A, Peterson N, Mulvey ME, Müller R-A (2013): Local
598 Functional Overconnectivity in Posterior Brain Regions Is Associated with
599 Symptom Severity in Autism Spectrum Disorders. *Cell Rep*. 5: 567–572.
600 19. Canolty RT, Knight RT (2010): The functional role of cross-frequency coupling.
601 *Trends Cogn Sci*. 14: 506–515.
602 20. Seymour RA, Rippon G, Kessler K (2017): The Detection of Phase Amplitude
603 Coupling during Sensory Processing. *Front Neurosci*. 11: 487.
604 21. Bonnefond M, Kastner S, Jensen O (2017): Communication between Brain
605 Areas Based on Nested Oscillations. *ENeuro*. 4: ENEURO–0153.
606 22. Mejias JF, Murray JD, Kennedy H, Wang X-J (2016): Feedforward and feedback
607 frequency-dependent interactions in a large-scale laminar network of the
608 primate cortex. *Sci Adv*. 2: e1601335.
609 23. Rubenstein JLR, Merzenich MM (2003): Model of autism: increased ratio of
610 excitation/inhibition in key neural systems. *Genes Brain Behav*. 2: 255–267.
611 24. Bastos AM, Vezoli J, Bosman CA, Schoffelen J-M, Oostenveld R, Dowdall JR, *et*
612 *al.* (2015): Visual Areas Exert Feedforward and Feedback Influences through
613 Distinct Frequency Channels. *Neuron*. 85: 390–401.
614 25. Michalareas G, Vezoli J, Van Pelt S, Schoffelen J-M, Kennedy H, Fries P (2016):
615 Alpha-beta and gamma rhythms subserve feedback and feedforward
616 influences among human visual cortical areas. *Neuron*. 89: 384–397.
617 26. Klimesch W (2012): Alpha-band oscillations, attention, and controlled access to
618 stored information. *Trends Cogn Sci*. 16: 606–617.
619 27. Richter CG, Thompson WH, Bosman CA, Fries P (2017): Top-down beta
620 enhances bottom-up gamma. *J Neurosci*. 3771–16.
621 28. Chacko RV, Kim B, Jung SW, Daitch AL, Roland JL, Metcalf NV, *et al.* (2018):
622 Distinct phase-amplitude couplings distinguish cognitive processes in human
623 attention. *NeuroImage*. 175: 111–121.
624 29. Spaak E, Bonnefond M, Maier A, Leopold DA, Jensen O (2012): Layer-specific
625 entrainment of gamma-band neural activity by the alpha rhythm in monkey
626 visual cortex. *Curr Biol*. 22: 2313–2318.
627 30. Dinstein I, Heeger DJ, Lorenzi L, Minshew NJ, Malach R, Behrmann M (2012):
628 Unreliable evoked responses in autism. *Neuron*. 75: 981–991.
629 31. Hillebrand A, Barnes GR (2005): Beamformer analysis of MEG data. *Int Rev*
630 *Neurobiol*. 68: 149–171.
631 32. Bastos AM, Litvak V, Moran R, Bosman CA, Fries P, Friston KJ (2015): A DCM
632 study of spectral asymmetries in feedforward and feedback connections
633 between visual areas V1 and V4 in the monkey. *Neuroimage*. 108: 460–475.

33. Raven JC, Court JH (1998): *Raven's progressive matrices and vocabulary scales*. Oxford Psychologists Press Oxford, UK.
34. Robertson AE, Simmons DR (2013): The relationship between sensory sensitivity and autistic traits in the general population. *J Autism Dev Disord*. 43: 775–784.
35. Baron-Cohen S, Wheelwright S, Hill J, Raste Y, Plumb I (2001): The "Reading the Mind in the Eyes" test revised version: A study with normal adults, and adults with Asperger syndrome or high-functioning autism. *J Child Psychol Psychiatry*. 42: 241–251.
36. Oakley BF, Brewer R, Bird G, Catmur C (2016): Theory of mind is not theory of emotion: A cautionary note on the Reading the Mind in the Eyes Test. *J Abnorm Psychol*. 125: 818.
37. Jenkinson M, Smith S (2001): A global optimisation method for robust affine registration of brain images. *Med Image Anal*. 5: 143–156.
38. Fischl B (2012): FreeSurfer. *Neuroimage*. 62: 774–781.
39. Essen V, C D, Glasser MF, Dierker DL, Harwell J, Coalson T (2012): Parcellations and Hemispheric Asymmetries of Human Cerebral Cortex Analyzed on Surface-Based Atlases. *Cereb Cortex*. 22: 2241–2262.
40. Taulu S, Simola J (2006): Spatiotemporal signal space separation method for rejecting nearby interference in MEG measurements. *Phys Med Biol*. 51: 1759.
41. Oostenveld R, Fries P, Maris E, Schoffelen J-M (2010): FieldTrip: open source software for advanced analysis of MEG, EEG, and invasive electrophysiological data. *Comput Intell Neurosci*. 2011. 1.
42. Van Veen BD, van Drongelen W, Yuchtman M, Suzuki A (1997): Localization of brain electrical activity via linearly constrained minimum variance spatial filtering. *IEEE Trans Biomed Eng*. 44: 867–880.
43. Glasser MF, Coalson TS, Robinson EC, Hacker CD, Harwell J, Yacoub E, *et al.* (2016): A multi-modal parcellation of human cerebral cortex. *Nature*. 536: 171–178.
44. Hoogenboom N, Schoffelen J-M, Oostenveld R, Parkes LM, Fries P (2006): Localizing human visual gamma-band activity in frequency, time and space. *Neuroimage*. 29: 764–773.
45. Dhamala M, Rangarajan G, Ding M (2008): Analyzing information flow in brain networks with nonparametric Granger causality. *Neuroimage*. 41: 354–362.
46. Granger CW (1969): Investigating causal relations by econometric models and cross- spectral methods. *Econom J Econom Soc*. 424–438.
47. Maris E, Oostenveld R (2007): Nonparametric statistical testing of EEG- and MEG-data. *J Neurosci Methods*. 164: 177–190.
48. Özkurt TE, Schnitzler A (2011): A critical note on the definition of phase–amplitude cross-frequency coupling. *J Neurosci Methods*. 201: 438–443.
49. Cohen MX (2008): Assessing transient cross-frequency coupling in EEG data. *J Neurosci Methods*. 168: 494–499.
50. Muthukumaraswamy SD (2013): High-frequency brain activity and muscle artifacts in MEG/EEG: a review and recommendations. *Front Hum Neurosci*. 7.
51. Spyropoulos G, Bosman CA, Fries P (2018): A theta rhythm in macaque visual cortex and its attentional modulation. *Proc Natl Acad Sci*. 201719433.
52. Capotosto P, Babiloni C, Romani GL, Corbetta M (2009): Frontoparietal cortex controls spatial attention through modulation of anticipatory alpha rhythms. *J*

Neurosci. 29: 5863–5872.
53. Palva S, Palva JM (2011): Functional roles of alpha-band phase synchronization in local and large-scale cortical networks. *Front Psychol*. 2: 204.
54. VanRullen R, Koch C (2003): Visual Selective Behavior Can Be Triggered by a Feed- Forward Process. *J Cogn Neurosci*. 15: 209–217.
55. Mottron L, Dawson M, Soulieres I, Hubert B, Burack J (2006): Enhanced perceptual functioning in autism: An update, and eight principles of autistic perception. *J Autism Dev Disord*. 36: 27–43.
56. Jobs EN, Falck-Ytter T, Bölte S (2018): Local and Global Visual Processing in 3-Year- Olds With and Without Autism. *J Autism Dev Disord*. 1–9.
57. Berman JI, Liu S, Bloy L, Blaskey L, Roberts TP, Edgar JC (2015): Alpha-to-gamma phase-amplitude coupling methods and application to autism spectrum disorder. *Brain Connect*. 5: 80–90.
58. Onslow ACE, Jones MW, Bogacz R (2014): A canonical circuit for generating phase- amplitude coupling. *PloS One*. 9: e102591.
59. Voytek B, Knight RT (2015): Dynamic network communication as a unifying neural basis for cognition, development, aging, and disease. *Biol Psychiatry*. 77: 1089–1097.
60. Hahamy A, Behrmann M, Malach R (2015): The idiosyncratic brain: distortion of spontaneous connectivity patterns in autism spectrum disorder. *Nat Neurosci*. 18: 302–309.
61. Mamashli F, Khan S, Bharadwaj H, Losh A, Pawlyszyn SM, Hämäläinen MS, Kenet T (2018): Maturational trajectories of local and long-range functional connectivity in autism during face processing. *Hum Brain Mapp*.
62. Friston K (2005): A theory of cortical responses. *Philos Trans R Soc Lond B Biol Sci*. 360: 815–836.
63. Palmer CJ, Lawson RP, Hohwy J (2017): Bayesian approaches to autism: Towards volatility, action, and behavior. *Psychological bulletin*. 143: 521.
64. Pellicano E, Burr D (2012): When the world becomes “too real”: a Bayesian explanation of autistic perception. *Trends Cogn Sci*. 16: 504–510.
65. Ashwin E, Ashwin C, Rhydderch D, Howells J, Baron-Cohen S (2009): Eagle-eyed visual acuity: an experimental investigation of enhanced perception in autism. *Biol Psychiatry*. 65: 17–21.
66. Loth E, Murphy DG, Spooren W (2016): Defining precision medicine approaches to autism spectrum disorders: concepts and challenges. *Front Psychiatry*. 7: 188.
67. Gohel B, Lim S, Kim M-Y, Kwon H, Kim K (2017): Approximate Subject Specific Pseudo MRI from an Available MRI Dataset for MEG Source Imaging. *Front Neuroinformatics*. 11: 50.
68. Nolte G (2003): The magnetic lead field theorem in the quasi-static approximation and its use for magnetoencephalography forward calculation in realistic volume conductors. *Phys Med Biol*. 48: 3637–3652.
69. Litvak V, Mattout J, Kiebel S, Phillips C, Henson R, Kilner J, *et al.* (2011): EEG and MEG data analysis in SPM8. *Comput Intell Neurosci*. 2011.
70. Van Essen DC, Ugurbil K, Auerbach E, Barch D, Behrens TEJ, Bucholz R, *et al.* (2012): The Human Connectome Project: a data acquisition perspective. *Neuroimage*. 62: 2222–2231.
71. Canolty RT, Edwards E, Dalal SS, Soltani M, Nagarajan SS, Kirsch HE, *et al.* (2006): High gamma power is phase-locked to theta oscillations in human neocortex. *Science*. 313: 1626–1628.

Supplementary Methods

Participant Exclusion

MEG data from a further 9 participants was collected but excluded, due to: intolerance to MEG (2 ASD); movement over 0.5cm (2 ASD, 2 control); metal artefacts (1 ASD, 1 control); AQ score over 30 (1 control).

MEG Acquisition

MEG data were acquired using a 306-channel Neuromag MEG system (Vectorview, Elekta, Finland) made up of 102 triplets of two orthogonal planar gradiometers and one magnetometer. All recordings were performed inside a magnetically shielded room at a sampling rate of 1000Hz. Five head position indicator (HPI) coils were applied for continuous head position tracking, and visualised post-acquisition using an in-house Matlab script. For MEG-MRI coregistration purposes three fiducial points, the locations of the HPI coils and 300-500 points from the head surface were acquired using the integrated Polhemus Fastrak digitizer. Visual stimuli were presented on a screen located 86cm from participants (resulting in 2 cycles/degree for the visual grating), and auditory feedback through MEG-compatible earphones.

Structural MRI

A structural T1 brain scan was acquired for source reconstruction using a Siemens MAGNETOM Trio 3T scanner with a 32-channel head coil (TE=2.18ms, TR=2300ms, TI=1100ms, flip angle=9°, 192 or 208 slices depending on head size, voxel-size = 0.8x0.8x0.8cm).

MEG-MRI Coregistration and 2D Cortical Mesh Construction

MEG data were co-registered with participants MRI structural scan by matching the digitised head-shape data with surface data from the structural scan (38). Two control participants did not complete a T1 structural MRI and therefore a pseudo-MRI was used, see (70) for full procedure. The aligned MRI-MEG images were used to create a forward model based on a single-shell description of the inner surface of the skull (71), using the segmentation function in SPM8 (72). The cortical mantle was then extracted to create a cortical mesh, using Freesurfer v5.3 (39), and registered to a standard fs_LR mesh, based on the Conte69 brain (Van Essen 2012), using an interpolation algorithm from the Human Connectome Project (Van Essen et al., 2012; instructions here: https://goo.gl/3HYA3L). Finally, the mesh was downsampled to 4002 vertices per hemisphere.

PAC

The mean vector length approach estimates PAC from a signal with length N, by combining phase (ϕ) and amplitude information to create a complex-valued signal: $f_a e^{i(\phi f_p)}$ (74), in which each vector corresponds to a certain time-point (n). If the resulting probability distribution function is non-uniform, this suggests a coupling between f_p and f_a, which can be quantified by taking the length of the average vector. As recommended by Özkurt & Schnitzler (2011) a normalisation factor was also applied corresponding to the power of f_a (50).

$$MI = \frac{1}{\sqrt{N}} \frac{\left|\frac{1}{N}\sum_{n=1}^{N} f_a(n) e^{i\left(\phi f_p(n)\right)}\right|}{\sqrt{\frac{1}{N}\sum_{n=1}^{N} f_a(n)^2}}$$

Supplementary Figures

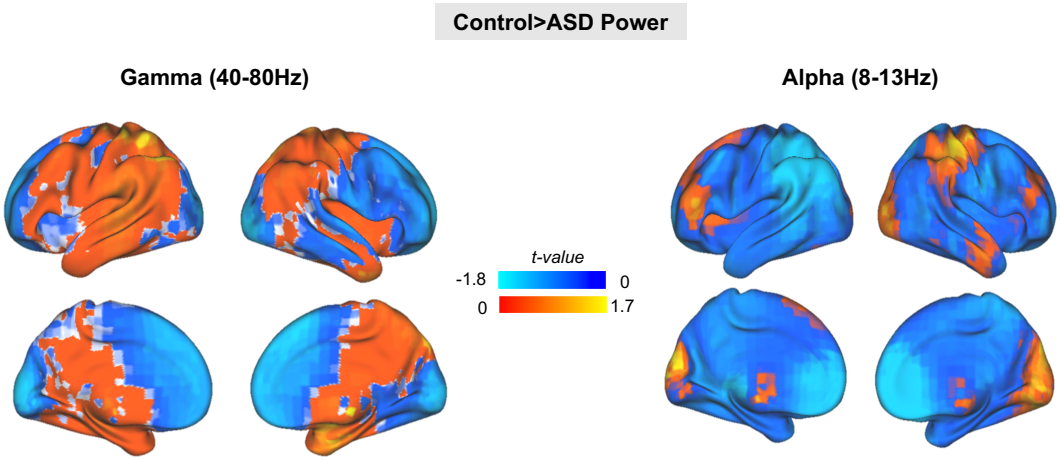

Figure S1: Brain-wide statistical comparison of control>ASD source-space oscillatory power for gamma (40-80Hz) and alpha (8-13Hz). There were no significant differences in either alpha or gamma power between groups (p>.05, corrected for multiple comparisons).

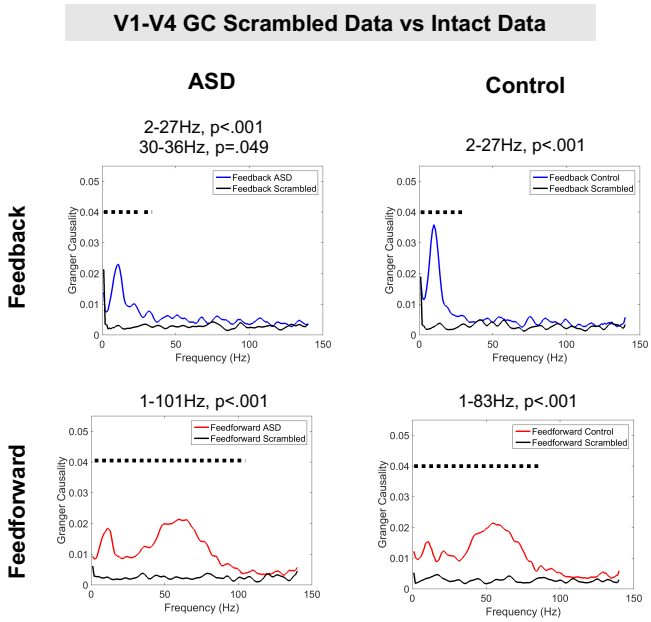

Figure S2: V1-V4 feedforward and V4-V1 Granger Causality (GC) values were statistically compared with GC values computed using scrambled V1/V4 data with same spectral properties as the intact data. On each sub-figure the black dotted line

signifies intact GC values significantly greater than scrambled GC values (p<.05). The exact frequency range and p-values are listed at the top of each plot.

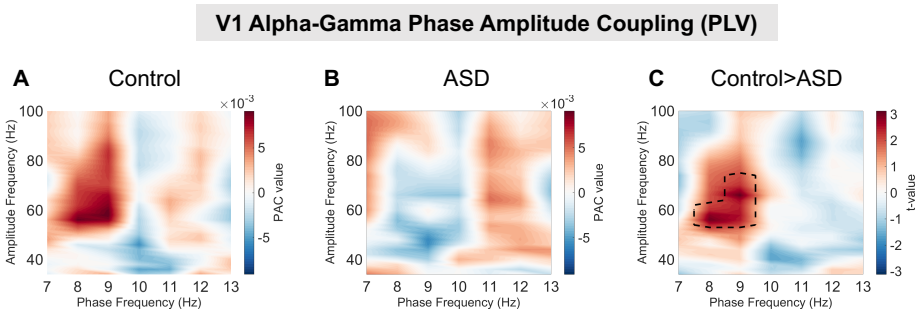

Figure S3: Alpha-Gamma Phase Amplitude Coupling in V1 was quantified using an alternative PLV approach (Cohen, 2008). (A-B) Both control and ASD group results show similar patterns of PAC changes compared with Figure 3A-B. (C) Statistical comparison of control>ASD indicated one positive cluster of increased PAC (p=.037) from 54-74Hz amplitude and 8-9Hz phase, replicating Figure 3C.

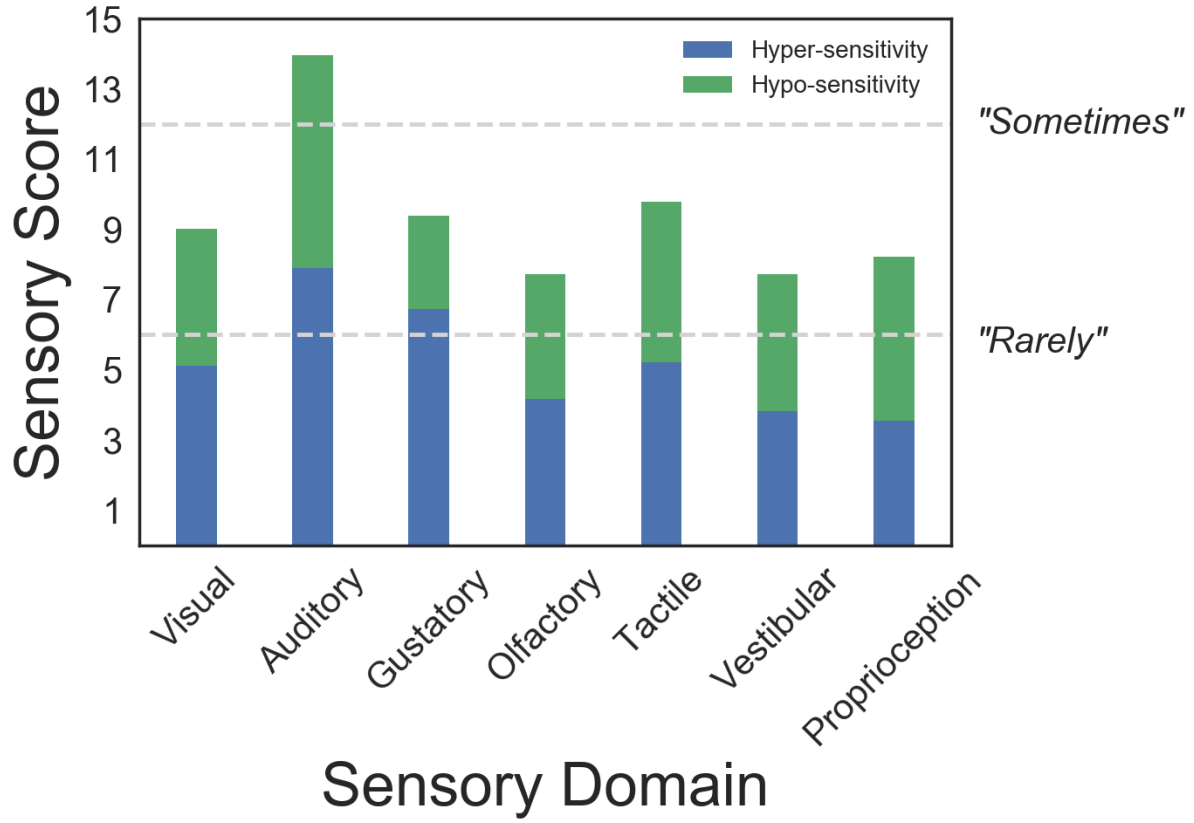

Figure S4: Responses to the Glasgow Sensory Questionnaire were grouped by sensory domain (maximum score = 20) and hypo- / hyper-sensitivity (green and blue bars respectively). Our data show a heterogeneous pattern of sensory symptoms, with mixture of hypo- and hyper-sensitivities. Visual symptoms scored 9.0/20 corresponding to questionnaire answers between “Rarely” and “Sometimes”. Auditory sensory symptoms were higher than for other modalities.